

DNArch: Learning Convolutional Neural Architectures by Backpropagation

David W. Romero^{*1} Neil Zeghidour²

Abstract

We present *Differentiable Neural Architectures* (DNArch), a method that jointly learns the weights and the architecture of Convolutional Neural Networks (CNNs) by backpropagation. In particular, DNArch allows learning (i) the size of convolutional kernels at each layer, (ii) the number of channels at each layer, (iii) the position and values of downsampling layers, and (iv) the depth of the network. To this end, DNArch views neural architectures as continuous multidimensional entities, and uses learnable differentiable masks along each dimension to control their size. Unlike existing methods, DNArch is not limited to a predefined set of possible neural components, but instead it is able to discover entire CNN architectures across all combinations of kernel sizes, widths, depths and downsampling. Empirically, DNArch finds performant CNN architectures for several classification and dense prediction tasks on both sequential and image data. When combined with a loss term that considers the network complexity, DNArch finds powerful architectures that respect a predefined computational budget.

1. Introduction

Convolutional Neural Networks (CNNs) (LeCun et al., 1998) are widely used for tasks such as image classification (Krizhevsky et al., 2012; He et al., 2016), speech recognition (Sercu et al., 2016; Zeghidour et al., 2018), text classification (Conneau et al., 2016) and generative modeling (Oord et al., 2016; Dhariwal & Nichol, 2021) due to their performance and efficiency. However, tailoring a CNN architecture to a specific task or dataset typically requires substantial human intervention and cross-validation to design the architectures, e.g. to determine appropriate kernel sizes, width, depth, etc.

This has motivated exploring the space of architectures in an automatic fashion, by developing architecture search al-

^{*}Work done while interning at Google. ¹Vrije Universiteit Amsterdam, The Netherlands. ²Google Research, Paris, France. Correspondence to: David W. Romero <d.w.romeroguzman@vu.nl>, Neil Zeghidour <neilz@google.com>.

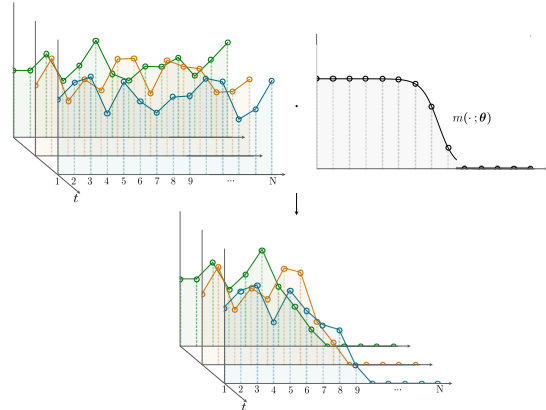


Figure 1. DNArch views neural architectures as if they were defined in a continuous multidimensional space, and uses learnable masks to learn their length by backpropagation. This example shows how DNArch learns the width of a layer by applying a differentiable mask $m(\cdot; \theta)$ to the channel dimension of the input. Different values of θ lead to a different number of channels.

gorithms (Zoph & Le, 2017; Liu et al., 2018a; Kandasamy et al., 2018). While these methods can find good architectures, they must solve an expensive discrete optimization problem that involves training and evaluating candidate architectures in each iteration, e.g. to optimize a reward with reinforcement learning (Zoph & Le, 2017), or to evolve the model through a genetic algorithm (Liu et al., 2018a). Differentiable Architecture Search (DARTS) (Liu et al., 2018b) addresses this issue by allowing the network to consider a set of *predefined* possible components in parallel, e.g., convolutions with kernels of size 3×3 , 5×5 , 7×7 , and adjusting their contribution using learnable weights (see Fig. 2). While this approach allows DARTS to *select* components via backpropagation, it (i) requires defining a small, finite set of possible components beforehand, and (ii) once an architecture is found, it must be retrained from scratch to remove the influence of other options on the output.

In this paper, we introduce *Differentiable Neural Architectures* (DNArch), a method that simultaneously learns the weights and the entire architecture of a CNN during training using backpropagation. That is, the weights as well as:

- The size of convolutional kernels at each layer,
- The number of channels at each layer,
- The position and resolution of downsampling layers, and
- The number of layers of the network.

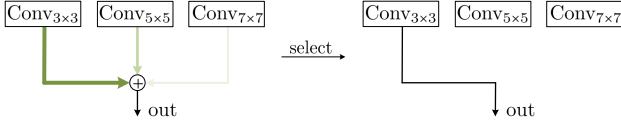


Figure 2. Use of DARTS to learn the size of convolutional kernels. DARTS uses backpropagation to select among predefined options.

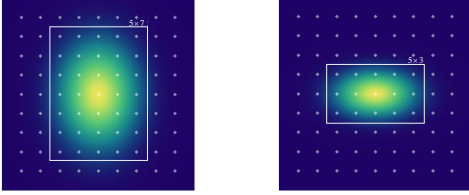


Figure 3. Use of DNArch to learn the size of convolutional kernels. By modifying the parameters of the differentiable mask $m(\cdot; \theta)$, convolutional kernels of different sizes can be obtained.

To this end, DNArch views neural architectures as if they were defined in a multidimensional continuous space—with dimensions corresponding to the network’s depth, width, etc.—, and uses differentiable masks with learnable parameters along each dimension to control their length (Fig. 1). As a result, unlike DARTS, DNArch does *not* require a predefined set of components to choose from, but instead is able to choose from *all* admissible values, e.g., all kernel sizes between 1×1 and $K_{\max} \times K_{\max}$. Note that, DNArch is truly continuous and does not require multiple instantiations of the same layer for different parameter values, e.g., Fig. 2. Instead, it is able to search across parameter values simply by modifying the learnable parameters of the mask (Fig. 3). Finally, as both the architecture and the weights are optimized over a single run, no finetuning step is needed.

Results. We show that DNArch is able to find performant CNN architectures for several classification and dense prediction tasks on sequential and image datasets. The architectures found by DNArch consistently surpass the general-purpose convolutional architecture on which DNArch is applied, and often outperform architectures specifically designed for each task. Furthermore, when combined with a loss term that controls the computational complexity of candidate networks, DNArch finds performant CNN architectures that adhere to a predefined computational budget.

To the best of our knowledge, DNArch is the first method that jointly learns the weights and the architecture of a CNN by backpropagation, exploring all combinations of kernel sizes, widths, depths and downsampling within a large admissible range.

2. Method

DNArch has two main components: Differentiable Masking and Continuous Kernel Convolutions. In this section, we introduce these concepts and show how they can be used to learn CNN architectures by backpropagation next.

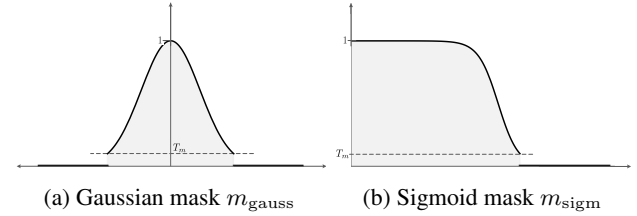
2.1. Differentiable Masking

Let us consider an arbitrary function $f : [a, b] \rightarrow \mathbb{R}$, which we want to be non-zero only in a subset $[c, d] \subseteq [a, b]$. To this end, we can multiply f with a mask m whose values are non-zero only on $[c, d]$, e.g., a rectangular mask $\Pi_{[c,d]}(x) = \{1 \forall x \in [c, d], 0 \text{ else}\}$. However, as its gradient is either zero or non-defined, it is not possible to learn the interval in which it is non-zero by backpropagation. To overcome this limitation, we can instead use a parametric differentiable mask $m(\cdot; \theta)$ whose interval of non-zero values is defined by its parameters θ . As the mask $m(\cdot; \theta)$ is differentiable with regard to its parameters θ , we can learn the interval on which it is non-zero using backpropagation.

In this work, we consider two types of masks: a Gaussian mask $m_{\text{gauss}}(\cdot; \mu, \sigma^2)$ parameterized by its mean and variance $\theta = \{\mu, \sigma^2\}$; and a Sigmoid mask $m_{\text{sigm}}(\cdot; \mu, \tau)$ parameterized by its offset and its temperature $\theta = \{\mu, \tau\}$:

$$m_{\text{gauss}}(x; \mu, \sigma^2) = \begin{cases} \bar{m} = \exp\left(-\frac{1}{2} \frac{(x-\mu)^2}{\sigma^2}\right) & \bar{m} \geq T_m \\ 0 & \text{else} \end{cases} \quad (1)$$

$$m_{\text{sigm}}(x; \mu, \tau) = \begin{cases} \bar{m} = 1 - \frac{1}{1 + \exp(-\tau(x-\mu))} & \bar{m} \geq T_m \\ 0 & \text{else} \end{cases} \quad (2)$$



where T_m is a predefined threshold below which the mask is zero. To avoid clutter, we refer to these masks as m_{gauss} and m_{sigm} and provide specific instantiations when needed.

Multidimensional masks. N-dimensional masks can be constructed by combining N 1D masks, each with their own parameters. For example, the Gaussian mask used to learn the size of convolutional kernels in Fig. 3 is constructed as:

$$m_{\text{gauss}}(x, y; \{\{\mu_X, \mu_Y\}, \{\sigma_X^2, \sigma_Y^2\}\}) \\ = m_{\text{gauss}}(x; \{\mu_X, \sigma_X^2\}) \cdot m_{\text{gauss}}(y; \{\mu_Y, \sigma_Y^2\})$$

2.1.1. RENDERING ONLY FOR NON-ZERO MASK VALUES

Parts of differentiable masks will map to zero based on the value of the parameters θ . Hence, it would be a waste of compute to render the mask—and the corresponding network parameters, e.g., channels $\text{ch} \in [10, N]$ in Fig. 1—to zero them out next. Luckily, we can take advantage of the invertible form of the Gaussian and Sigmoid masks to render only values for which the mask is non-zero. To this end, we find the value x_{T_m} for which the mask is equal to the threshold T_m , i.e., $x_{T_m} = x \mid m(x; \theta) = T_m$, and only render the mask and the corresponding network parameters for values of x for which the value of the mask is greater than T_m . By

inverting the mask equations (Eqs. 1, 2), we obtain x_{T_m} as:

$$\pm x_{T_m} = \mu \pm \sqrt{-2\sigma^2 \log(T_m)}, \text{ and} \quad (3)$$

$$x_{T_m} = \mu - \frac{1}{\tau} \log\left(\frac{1}{1 - T_m} - 1\right), \quad (4)$$

for the Gaussian and Sigmoid masks, respectively. Consequently, we can make sure that all rendered values will be used by only rendering the mask and related network parameters for x values within the range $[-x_{T_m}, x_{T_m}]$ for Gaussian masks and $[x_{\min}, x_{T_m}]$ for Sigmoid masks, where x_{\min} depicts the lowest coordinate indexing the mask.

2.2. Continuous Kernel Convolutions

To prevent finding poor architectures due to insufficiently large receptive fields, it is important for a network to be able to model the global context regardless of specific architectural choices. We rely on Continuous Kernel Convolutions (CKConvs) (Romero et al., 2021b) to model (global) long range dependencies on inputs of arbitrary length, resolution and dimensionality regardless of the network architecture.

CKConvs view convolutional kernels ψ as continuous functions parameterized by a small neural network $\text{MLP}_\psi: \mathbb{R}^D \rightarrow \mathbb{R}^{N_{\text{in}} \times N_{\text{out}}}$ that receives coordinates $\mathbf{c}_i \in \mathbb{R}^D$ as input and predicts the value of the convolutional kernel at those coordinates: $\mathbf{c}_i \mapsto \text{MLP}_\psi(\mathbf{c}_i) = \psi(\mathbf{c}_i)$. To construct a kernel of size $K_x \times K_y$, a CKConv layer constructs a grid of $K_x \times K_y$ coordinates $[\mathbf{c}_{(1,1)}, \mathbf{c}_{(1,2)}, \dots, \mathbf{c}_{(K_x, K_y)}]$, and passes each coordinate through the neural network MLP_ψ (Fig. 6). CKConvs construct large kernels with few parameters by detaching the size of the kernel from its parameter count.

2.3. The need for learnable architectures

General-purpose architectures like Perceiver (Jaegle et al., 2021) and the Continuous CNN (CCNN) (Romero et al., 2022) make few assumptions about their input signals and thus require few architectural changes to handle different tasks. However, general-purpose architectures are static, and thus they will likely not be optimal for all tasks considered. For instance, the Perceiver maps inputs to a hidden representation of constant size regardless of the complexity of the task and the input length, resolution and dimensionality. Consequently, it may not correctly represent tasks with high difficulty or on large inputs. CCNNs, on the other hand, avoid pooling and always perform (global) convolutions on the original input resolution. While this addresses the issue of having a hidden representation of fixed size for inputs with different characteristics, CCNNs can lead to unnecessarily high computational complexity by always performing convolutions at the input resolution. In addition, both the architectures of Perceivers and CCNNs are static, and thus they are unable to adapt to tasks of varying difficulty.

To address these limitations, we instead propose to construct CNN architectures able to automatically tune themselves to fit the requirements of a particular task.

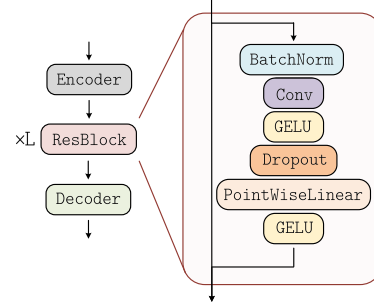


Figure 5. The Continuous CNN architecture (Romero et al., 2022).

2.4. Learning CNN architectures by backpropagation

Most components of DNArch, such as the learning of the network’s width and depth, are not limited to convolutional architectures. However, this research aims to show how DNArch can be used to learn as many components of a neural architecture as possible. To that end, we use a general-purpose convolutional architecture: the Continuous CNN, and make all its architectural components learnable.

The Continuous CNN (CCNN) is a general-purpose convolutional model able to handle inputs of arbitrary dimension, length and resolution without changes. It consists of an Encoder, a Decoder, and many residual blocks (Fig. 5). The Encoder and Decoder adapt the input and output of the model to the goal of the task, e.g., dense / global predictions. We refer to the branch on which residual blocks modify the input as *residual branch*, and to the branch connecting the input and the output directly as the *identity branch*. Importantly, the CCNN’s ability to consider global context on inputs of any dimension makes it an ideal base network for DNArch. It prevents the formation of poor architectures due to insufficient receptive fields and allows DNArch to be used on 1D and 2D data without modifying the base network.

2.4.1. KERNEL SIZES

Differentiable Masking can be combined with Continuous Kernel Convolutions to learn the size of convolutional kernels by backpropagation. This is done by modelling convolutional kernels as the product of a small neural network MLP_ψ , i.e., a Continuous Kernel Convolution, and a differentiable mask $m(\cdot; \theta)$ with learnable parameters, i.e., $\psi(\mathbf{c}_i) = \text{MLP}_\psi(\mathbf{c}_i) \cdot m(\mathbf{c}_i; \theta)$ (Fig. 6). Importantly, we can construct the convolutional kernel only for values where the mask $m(\mathbf{c}_i; \theta)$ is non-zero as outlined in Sec. 2.1.1.

2.4.2. DOWNSAMPLING

Differentiable Masking can also be used to learn downsampling by applying a differentiable mask on the Fourier domain. The Fourier transform \mathcal{F} represents a function $f: \mathbb{R}^D \rightarrow \mathbb{R}$ in terms of its frequency components $\tilde{f}: \mathbb{R}^D \rightarrow \mathbb{C}$ —its spectrum— which map frequencies ω to the “amount” of that frequency in the input function f ; $\mathcal{F}[f]: \omega \mapsto \tilde{f}(\omega)$. Once the function is represented on the Fourier domain, one can directly modify the “amount” of a particular frequency

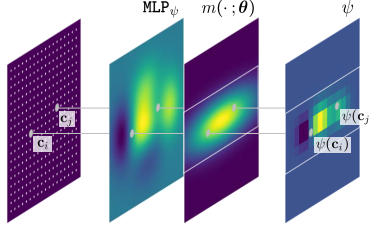


Figure 6. Learning kernel sizes with Differentiable Masking. First introduced in FlexConv (Romero et al., 2021a), we model convolutional kernels as the combination of a CKConv and a differentiable mask. The CKConv defines the functional form of the kernel, and the differentiable mask controls its size.

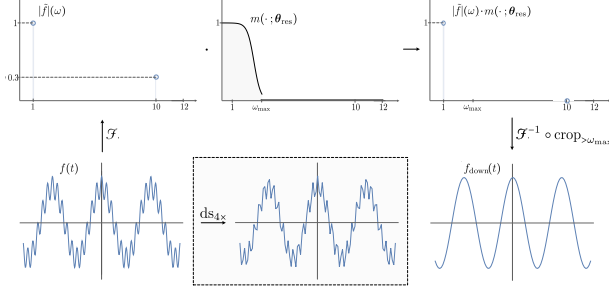


Figure 7. Learning downsampling with Differentiable Masking. To downsample a signal f , we multiply its spectrum $\tilde{f}=\mathcal{F}[f]$ with a differentiable mask $m(\omega; \theta_{\text{res}})$, crop the resulting low-passed spectrum above the cutoff frequency ω_{max} , and convert it back to the spatial domain next. It is important to note that not considering the spectral content during downsampling leads to *aliasing*, where the final resolution is insufficient to accurately represent the underlying signal (middle down). This is problematic as observed by previous work (Zhang, 2019; Karras et al., 2021).

ω in the input by modifying its amplitude $\tilde{f}(\omega)$.

Low-pass filtering is a technique widely used in signal processing to remove high frequencies components from a signal. It is accomplished by multiplying the signal’s spectrum with a mask m whose values above the cutoff frequency ω_{max} are zero. A consequence of low-pass filtering is that the resulting signal can be represented at a lower resolution determined by ω_{max} without loss of information as:

$$f_{\text{down}}=\mathcal{F}^{-1}\left[\text{crop}_{>\omega_{\text{max}}}(\mathcal{F}[f]\cdot m)\right], \quad (5)$$

where \mathcal{F} , \mathcal{F}^{-1} are the Fourier and inverse Fourier transform respectively, f_{down} represents the downsampled signal, and $\text{crop}_{>\omega_{\text{max}}}$ is an operator that crops all values above ω_{max} .

By making the mask m learnable, the network can determine which frequencies are important at a particular layer, and use this information to do downsampling (Fig. 7).

Computational implications of the Fourier convolution.

The *Fourier convolution theorem* states that the convolution between a function f and a convolutional kernel ψ is equivalent to the pointwise multiplication of their Fourier transforms $\mathcal{F}[f]$, $\mathcal{F}[\psi]$. This means that we can compute a convolution by taking the Fourier transform of both signals, multiplying them in the Fourier domain, and then transform-

ing them back to the spatial domain:

$$(f * \psi)=\mathcal{F}^{-1}\left[\mathcal{F}[f]\cdot \mathcal{F}[\psi]\right]. \quad (6)$$

The computational complexity of this method is $L \log(L)$, which is faster than the complexity of a standard convolution ($L \cdot K$) when $K > \log(L)$. This is why Fourier convolutions are widely used in methods that rely on global convolutions, e.g., CKConv (Romero et al., 2021b), S4 (Gu et al., 2021).

Positioning of learnable downsampling. Fourier and inverse Fourier transforms are already being used in CNNs to compute convolutions. Hence, we can avoid recomputing these steps by placing the learnable downsampling operation *within* the convolution as follows:

$$(f * \psi)_{\text{down}}=\mathcal{F}^{-1}\left[\text{crop}_{>\omega_{\text{max}}}(m(\cdot; \theta)\cdot \mathcal{F}[f]\cdot \mathcal{F}[\psi])\right], \quad (7)$$

that is by applying the differentiable mask and the cropping operations before going back to the spatial domain.¹

Avoiding unnecessary rendering during downsampling.

Eq. 7 computes the convolution on the resolution of the input and downsamples next. However, we can invert this order of operations by using the approach in Sec. 2.1.1 to compute the convolution at the resolution determined by the mask. Note that the cutoff frequency of the mask is the coordinate at which the mask equals the threshold T_m , i.e., $\omega_{\text{max}}=x_{T_m}$. Hence, by using Eqs. 3, 4 we can find the cutoff frequency of the mask, which defines the minimum resolution required to faithfully represent the input. By downsampling both the input and convolutional kernel to that resolution before the convolution, it is effectively computed at that resolution.

Learning subsampling for dense tasks. We could tie the identity branch to use the same amount of downsampling as in the convolutional layer as Riad et al. (2022). However, this would limit the resolution of all representations after that specific block, which is undesirable for two reasons.

First, since we learn the entire network architecture during training, it is not known a priori what kind of processing will occur at each layer. Hence, later layers may need to work at higher resolution than previous ones. If we force the identity branch to have the same resolution as the corresponding convolutional layer, the resolution of subsequent layers will be limited by the previous residual block. Additionally, some tasks require the learned architecture to produce dense predictions, e.g., segmentation. In such cases, it is important for the output of the network to have the same resolution as the input, which becomes an issue if feature representations at the output of the network are of lower resolution.

¹The Fourier transform is not required for learning downsampling, e.g., for CNNs that do not use global kernels. As multiplication in the Fourier domain is equivalent to a convolution in the spatial domain, masking in the Fourier domain can be done on the spatial domain by taking the inverse Fourier transform of the mask, and convolving it with the input next (Appx. B).

Base on these observations, we perform downsampling *only* on the residual branch and upsample features at the end of the residual block to the resolution of the input. This allows us to (i) have features at the end of the network at the same resolution as the input and (ii) to learn U-Net like architectures (Ronneberger et al., 2015).

2.4.3. WIDTH

To learn the width of a layer, we apply a differentiable mask $m(\cdot; \theta)$ along the channel dimension of feature representations as shown in Fig. 1. The network can then adjust the number of channels of its hidden representations by learning the parameters θ . Note that we can use the approach in Sec. 2.1.1 to only render the channels that will be used.

Positioning of the width masks. We are interested in learning the width of all layers in a network. To this end, we apply differentiable masks with independent learnable parameters along the channel dimensions of all the network components that change the network’s width, i.e., all Conv and PWLinear layers. This corresponds to learning three independent masks for each residual block in the network, which correspond to the input (N_{in}), middle (N_{mid}) and output (N_{out}) channels of the block (Fig. 8). Components that do not change the width, e.g., BatchNorm, GELU, have their width determined by the preceding differentiable mask.

The advantage of avoiding masks on the identity branch.

Applying a differentiable mask on the output of the entire residual block to constrain its width, i.e., after the sum of the residual and identity branches, would accumulate the effect of all masks applied before that block. As a result, the l -th block would be effectively masked by the combination of all masks before that block, i.e., $\prod_{i \leq l} m_i$, with m_i the mask after the i -th block. Since the values of the masks live in the $[0, 1]$ interval, this would result in an exponential decrease in the magnitude of the hidden feature presentations. To avoid this, we apply the masks on the residual branch only. In addition, keeping the identity branch intact allows DNArch to construct DenseNet-like architectures (Huang et al., 2017), where blocks can reuse channels that only have been modified by some –or none– of the previous blocks.

2.4.4. DEPTH

We use Differentiable Masking to learn the network’s depth by viewing the number of intermediary blocks as a continuous axis with values $[1, 2, \dots, D]$ corresponding to the index of each block and using a differentiable mask $m(\cdot, \theta)$ along this axis to dynamically mask out some residual blocks based on the value of the mask parameters θ (Fig. 9).

Positioning of the depth mask. We apply the mask *only* on the residual branch to ensure that information can flow from the input to the output of the network regardless of the current mask parameters. Note that if the mask were applied on the identity branch, it would risk zeroing out feature

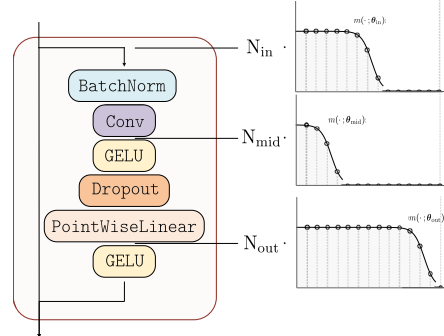


Figure 8. Positioning of masks for the learning of the width.

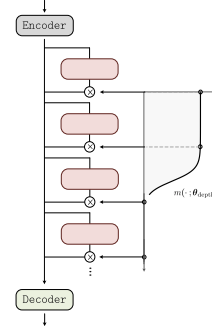


Figure 9. Learning the depth of the network with Differential Masking. By applying a differentiable mask with learnable parameters θ along the depth axis, some blocks can be dynamically masked out, allowing the network to adjust its depth during training.

representations at the end of the network at which point the network would only be able to output random predictions.

2.4.5. PUTTING IT ALL TOGETHER

By using the techniques described in Sections 2.4.1-2.4.4, DNArch uses backpropagation to learn both the weights and

- The size of convolutional kernels at each layer,
- The number of channels at each layer,
- The position and resolution of downsampling layers, and
- The depth of a CNN.

2.5. Learning CNN architectures under computational constraints

We can ensure that architectures found by DNArch meet a predefined complexity by including an additional loss term \mathcal{L}_{comp} that reflects the complexity of the network based on the current mask parameters. We define the optimization loss \mathcal{L} as the sum of the task objective loss \mathcal{L}_{obj} and the complexity loss \mathcal{L}_{comp} weighted by a factor λ :

$$\mathcal{L} = \mathcal{L}_{obj} + \lambda \mathcal{L}_{comp}. \quad (8)$$

By minimizing this loss, the optimization is encouraged to find architectures that meet the desired computational budget while still achieving good performance on the task.

2.5.1. DEFINING THE COMPLEXITY LOSS \mathcal{L}_{comp}

The purpose of \mathcal{L}_{comp} is to use the size of the learned masks to estimate the total computation needed for a forward pass of the network. Its construction is outlined below.

Layer-wise complexities. Let $C_{layer}(L, N_{in}, N_{out})$ be the number of operations required in a given layer with an

input of length L and N_{in} and N_{out} input and output channels. To estimate the number of computations required based on the current size of the masks, we can substitute the standard values with the size of the corresponding masks: $C_{\text{layer}}(\text{size}(m_{\text{res}}), \text{size}(m_{N_{\text{in}}}), \text{size}(m_{N_{\text{out}}}))$.

As an example, consider a pointwise linear layer. A pointwise linear layer $\text{lin} : \mathbb{R}^{N_{\text{in}}} \rightarrow \mathbb{R}^{N_{\text{out}}}$ takes an input f of length L and N_{in} number of channels and multiplies each element along the spatial dimensions of the input with a matrix of dimensions $[N_{\text{in}}, N_{\text{out}}]$ to produce an output of the same length, but with N_{out} number of channels. The total number of operations required in this layer is given by:

$$C_{\text{lin}}(f) = L \cdot N_{\text{in}} \cdot N_{\text{out}}.$$

Now, let us use three differentiable masks m_{res} , $m_{N_{\text{in}}}$ and $m_{N_{\text{out}}}$ to mask the resolution, input and output channels of the linear layer. The total number of computations is now:

$$C_{\text{lin,masked}} = \text{size}(m_{\text{res}}) \cdot \text{size}(m_{N_{\text{in}}}) \cdot \text{size}(m_{N_{\text{out}}}).$$

Since the size of the masks is now involved in the computation of the number of operations required, we can utilize the total number of operations as an additional source of feedback for updating the masks by making the function size differentiable with regard to the mask parameters.

The same concept is used to calculate the number of operations for other layers. A summary can be found in Appx. C.

Effect of the depth mask. To take into account the effect of the depth mask, we use it to determine the number of residual blocks in the network. If the number of operations of a network with D residual blocks is denoted as $C_{\text{net},D}$, the complexity of a network with masked depth is given by $C_{\text{net,size}(m_{\text{depth}})}$ with $\text{size}(m_{\text{depth}})$ the size of the mask.

Computing the size of the masks. The size of a mask can be calculated in a differentiable manner by determining the length of the mask in continuous space and using that length to estimate the change in size of the corresponding network dimension. Specifically, the length at a time t is $2x_{T_m}$ and $x_{T_m} - x_{\text{min}}$, for Gaussian and Sigmoid masks, respectively. For some initial $x_{T_m}^0$ and corresponding length N , the size of a Gaussian and a Sigmoid mask at time t is respectively:

$$\text{size}(m_{\text{gauss}}) = \frac{2x_{T_m}^t}{2x_{T_m}^0} N, \quad \text{and} \quad (9)$$

$$\text{size}(m_{\text{sigm}}) = \frac{x_{T_m}^t - x_{\text{min}}}{x_{T_m}^0 - x_{\text{min}}} N. \quad (10)$$

Computational constraints as an additional loss. Let C_{curr} be the current complexity of the network and C_{target} be the desired target complexity. We define the computational loss $\mathcal{L}_{\text{comp}}$ as the relative ℓ^2 difference between the relative complexity of the current network and the target:

$$\ell^2 \left(\frac{C_{\text{curr}}}{C_{\text{target}}}, 1 \right) = \left\| \frac{C_{\text{curr}}}{C_{\text{target}}} - 1.0 \right\|_2^2. \quad (11)$$

This form has two advantages over the alternative form $\ell^2(C_{\text{curr}}, C_{\text{target}})$. It prevents overflow that might occur when comparing large values $-C_{\text{curr}}$ and C_{target} can easily be in the range of $1e^{10}$, and it allows for consistent tuning of λ for different tasks and complexities. In the other form, λ also may need to be tuned for different complexity regimes.

3. Experiments

We evaluate DNArch on sequential and image datasets for classification and dense prediction tasks. On 1D, we use the Long Range Arena (LRA) benchmark (Tay et al., 2020), which includes six sequence modelling tasks with sequence lengths ranging from 1024 to over 16000. On 2D, we perform image classification on the CIFAR10 and CIFAR100 datasets (Krizhevsky et al., 2009) and report results on two dense prediction tasks from the NAS-Bench-360 benchmark (Tu et al., 2022): the DarcyFlow (Li et al., 2020) and Cosmic (Zhang & Bloom, 2020) tasks. A detailed description of the datasets used can be found in Appx. D.

Experimental setup. We use a $\text{CCNN}_{4,140}$ – a CCNN with 4 blocks and 140 channels – as base architecture and use DNArch to learn its architecture components. To understand the impact of learning each component, we also report results for a $\text{CCNN}_{4,140}$ without any learnable components and global convolutional kernels. We use a Gaussian mask to learn kernel sizes as Romero et al. (2021a), and Sigmoid masks to learn width, depth and downsampling. All masks use a threshold of $T_m=0.1$. The kernel size masks are initialized to be small and centered ($\mu=0$, $\sigma=0.0325$), resolution masks are initialized to weight the highest input frequency by 0.85 –via Eq. 4–, and the width and depth masks are initialized to match the base network. More information on hyperparameters, training regimes, and experimental settings can be found in Appx. E.

Nomenclature. We use the symbol DNArch as an operator acting on a base architecture and specify the learned components with indices K, R, W, D representing kernel sizes, resolutions, width and depth, respectively. For example, $\text{DNArch}_K(\text{CCNN}_{4,140})$ refers to using DNArch to learn only the kernel sizes of a $\text{CCNN}_{4,140}$.

3.1. DNArch without computational constraints

First, we use DNArch to improve the modeling capacity and computational efficiency of a $\text{CCNN}_{4,140}$. We achieve the former by using DNArch to adjust the receptive field of each layer. Next, we simultaneously learn kernel sizes and downsampling to enhance both the modeling capacity and computational complexity of the $\text{CCNN}_{4,140}$. It is worth noting that in this scenario, the term $\mathcal{L}_{\text{comp}}$ is not used, and the learning is solely driven by the objective loss \mathcal{L}_{obj} . Also, we only use Fourier convolutions in our experiments, meaning that the learned kernel sizes do not have an impact on the computational efficiency of the model.

Table 1. Performance on the LRA benchmark. × denotes random guessing. Highest per-section scores are in bold and the overall best scores are underlined. For DNArch, values in parenthesis indicate the computational cost of the architecture relative to the target complexity.

MODEL	LISTOPS	TEXT	RETRIEVAL	IMAGE	PATHFINDER	PATH-X	AVG.
Transformer (Vaswani et al., 2017)	36.37	64.27	57.46	42.44	71.40	×	53.66
Reformer (Kitaev et al., 2020)	37.27	56.10	53.40	38.07	68.50	×	50.56
Performer (Choromanski et al., 2020)	18.01	65.40	53.82	42.77	77.05	×	51.18
BigBird (Zaheer et al., 2020)	36.05	64.02	59.29	40.83	74.87	×	54.17
Mega ($\Theta(L^2)$) (Ma et al., 2022)	63.14	90.43	91.25	90.44	96.01	97.98	88.21
Mega-chunk ($\Theta(L)$) (Ma et al., 2022)	58.76	90.19	90.97	85.80	94.41	93.81	85.66
S4D (Gu et al., 2022)	60.47	86.18	89.46	88.19	93.06	91.95	84.89
S4 (Gu et al., 2021)	59.60	86.82	90.90	88.65	94.20	96.35	86.09
S5 (Smith et al., 2022)	61.50	89.31	91.40	88.00	95.33	98.58	87.35
FNet (Lee-Thorp et al., 2021)	35.33	65.11	59.61	38.67	77.80	×	54.42
Luna-256 (Ma et al., 2021)	37.25	64.57	79.29	47.38	77.72	×	59.37
CCNN _{4,140} (Romero et al., 2022)	44.85	83.59	×	87.62	91.36	×	76.86
CCNN _{4,140} (Global Kernels)	55.65	87.80	90.55	85.51	94.26		
DNArch _K (CCNN _{4,140})	59.90	88.28	90.66	86.07	93.46	89.93	84.72
DNArch _{K,R} (CCNN _{4,140})	60.15 _(0.80×)	88.50 _(0.75×)	91.08 _(0.78×)	86.55 _(0.82×)	94.05 _(0.89×)		
DNArch _{K,R,W,D} (CCNN _{4,140})	60.55 _(1.01×)	89.03 _(1.00×)	91.22 _(1.02×)	87.20 _(1.02×)	94.95 _(1.00×)	91.71 _(1.01×)	85.78

Table 2. Performance on Dense Tasks of NAS-Bench-360.

MODEL	DARCYFLOW rel. l^2 loss	COSMIC 1 - AUROC
Expert*	0.008	0.13
WRN (Zagoruyko & Komodakis, 2016)	0.073	0.24
DenseNAS (Fang et al., 2020)	0.100	0.38
DARTS (Liu et al., 2018b)	0.026	0.229
Auto-DL (Liu et al., 2019)	0.049	0.495
DASH (Shen et al., 2022)	0.060	0.190
CCNN _{4,140} (Global Kernels)	0.002989	0.059
DNArch _K (CCNN _{4,140})	0.002970	0.058
DNArch _{K,R} (CCNN _{4,140})	0.002929 _(0.79×)	0.056 _(0.82×)
DNArch _{K,R,W,D} (CCNN _{4,140})	0.002285 _(1.01×)	0.055 _(1.01×)

* FNO (Li et al., 2020) and deepCR (Zhang & Bloom, 2020).

Results. Except for the PathFinder and Path-X tasks, we find that using DNArch to learn kernel sizes consistently improves the accuracy of the base architecture (DNArch_K models in Tabs. 1-3). Interestingly, the resulting architectures perform on par, and even surpass, architectures specifically designed for each tasks without adjusting the underlying architecture, e.g., S4 (Gu et al., 2021) for sequential tasks and NFOs (Li et al., 2020) for PDEs on 2D. This is in contrast to existing NAS/DARTS methods, which require different base architectures to handle data with different characteristics. For instance, DASH (Shen et al., 2022) manually selects a base TCN (Bai et al., 2018) for sequential data and a base ResNet for image data to match the dimensionality of the input of each task.

When learning downsampling (DNArch_{K,R} models in Tabs. 1-3), DNArch improves the computational efficiency of the resulting models and often leads to slight accuracy improvements. The latter is due to lower resolution kernels being easier to model and learn than higher resolution ones.

3.2. DNArch with computational constraints

Next, we utilize DNArch to learn the entire neural architecture of a CCNN by starting with a base CCNN_{4,140} and allowing DNArch to learn its width, depth, kernel sizes and downsampling layers, while ensuring that the overall complexity of the new architecture is the same as the base model.

Table 3. Performance on Image Classification Datasets.

MODEL	CIFAR10	CIFAR100
CCNN _{4,140} (Global Kernels)	90.52	64.72
DNArch _K (CCNN _{4,140})	92.51	69.01
DNArch _{K,R} (CCNN _{4,140})	92.77 _(0.82×)	68.96 _(0.85×)
DNArch _{K,R,W,D} (CCNN _{4,140})	93.47 _(1.01×)	72.98 _(1.05×)

As in the previous case, our experiments only use Fourier convolutions and thus, the kernel sizes learned by DNArch do not affect the computational efficiency of the model.

Results. Our results (DNArch_{K,R,W,D} models in Tabs. 1-3) show that DNArch finds neural architectures with higher accuracy than the base CCNN_{4,140} while keeping the same computational complexity across all datasets. This shows the effectiveness of DNArch when working under computational constraints. Note that, once again, DNArch automatically discovers architectures that perform comparably or better than architectures specifically designed for each task.

Behaviour of the relative complexity during training.

Fig. 10 displays how the relative complexity (C_{curr}/C_{target}) changes during training on the Text dataset. DNArch is seen to search for neural architectures whose complexity stays near the target complexity throughout the entire training process. This behavior is consistent across all datasets.

3.3. Architectures found by DNArch

The architectures found by DNArch are listed in Tabs. 4, 5. We observe that the architectures found by DNArch display a wide range of diversity in terms of the learned components, even within each architecture. For instance, some residual blocks have a bottleneck structure, some an inverted bottleneck structure, and others have monotonically decreasing or increasing widths. Moreover, the resolution of found architectures for classification tasks, e.g., Text, often follow the style of U-Nets, and not the monotonically decreasing pattern commonly seen in handcrafted architectures. On dense tasks, we even observe architectures that resemble concatenated U-Nets, such as the concatenated U-Net like

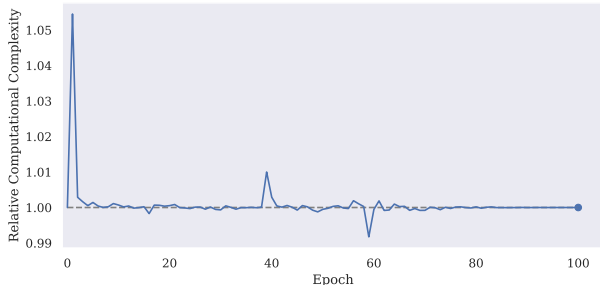


Figure 10. Evolution of the relative complexity ($C_{\text{curr}}/C_{\text{target}}$) during training on the Text task. DNArch moves across architectures with the same complexity through the course of training.

architecture found for the Cosmic task.

The kernel sizes found by DNArch are also very diverse. In 1D tasks, found kernels are often very large, which would make them parameter intensive with traditional convolutional kernel parameterizations. In 2D tasks, we often see rectangular kernels that do not follow a monotonic pattern of increasing or decreasing sizes. Instead, found architectures often perform interleaved low-level and high-level feature extraction. This behaviour can be seen in the human visual system, which iteratively uses global information to modify low-level representations, and refined low-level representations to modify previous global representations (Kietzmann et al., 2019). This resemblance is also observed in the cyclic U-Net like architectures found by DNArch.

4. Limitations

Training on TPU requires static shapes. We train our models on TPUs, a type of accelerator that requires a static computational graph derived for specific input and network shapes via the XLA (Accelerated Linear Algebra) compiler. As a result, TPUs do not support operations that change the shapes of arrays during training. This means that on TPUs, DNArch can only perform virtual modifications to the network during training, i.e., setting certain channels to zero but still computing their outputs. At inference, however, the masks are fixed. Consequently, we can effectively trim unused values, e.g., channels and layers, to remove useless computations in a way that is compatible with tt XLA.

It is important to note that this limitation is solely an implementation issue caused by nature of TPUs’ hardware and can be avoided by using libraries and hardware that support dynamic computational graphs, such as PyTorch and GPUs. While our results were obtained using TPUs, we will also provide a PyTorch implementation of DNArch that avoids this issue, making it more flexible and accessible, especially in scenarios where it is required to keep candidate networks close to the target complexity C_{target} during training.

DNArch requires instantiating the largest possible ar-

chitecture. While masking weights through a gradient update is straightforward, instructing the model to increase the number of active weights requires those weights to be instantiated so that the mask can access them when applied. This means that even when using dynamic computations, it is necessary to instantiate the largest possible architecture learnable by DNArch in memory. To overcome this limitation, we set a maximum limit for the network size along the depth and width dimensions as double the number of blocks and channels of the initial network, i.e., a CCNN_{8,280} and use the masks to initialize it as a CCNN_{4,140}. This allows DNArch to grow the number of channels and layers if necessary to find the optimal architecture within that range.

5. Outlook and future work

Input-dependent neural architectures. In this work, we keep the mask parameters constant for all inputs within a task. However, an alternative approach could use an additional neural network MLP_{mask} to predict the mask parameters based on the current input. This would enable the creation of input-dependent neural architectures similar to early-exit systems (Teerapittayanon et al., 2016; Ghodrati et al., 2021; Schuster et al., 2022), but where all aspects of the network architecture are input-dependent, i.e., width, depth, etc., providing a finer control of per-sample complexity than existing methods.

Dynamic weighting of $\mathcal{L}_{\text{comp}}$ during training. DNArch looks for neural architectures whose complexity stays near the target complexity throughout the entire training process (Fig. 10). This is a result of using a constant λ in Eq. 8. Alternatively, one could use a dynamic value of λ during training to induce a different training behaviors. For example, gradually increasing the value of λ would allow DNArch to explore architectures in a wider complexity range at first, and converge to a more efficient architecture afterwards, thus performing architecture search and distillation simultaneously, or finding the minimal architecture that reaches a performance threshold.

DNArch with additional objectives. Here, we only consider computational complexity when training with DNArch. However, one could add other loss components to promote finding neural architectures that meet other properties, e.g., memory efficiency, hardware-awareness and robustness.

Are handcrafted architectures optimal? Our results raise the question of whether current handcrafted architectures are truly optimal or rather a result of discrete parameterizations and predefined downsampling / upsampling steps in the architectures. Further analysis of the patterns exhibited by DNArch could provide deeper insights into what makes a neural architecture effective and how to construct them.

References

- Bai, S., Kolter, J. Z., and Koltun, V. An empirical evaluation of generic convolutional and recurrent networks for sequence modeling. *arXiv preprint arXiv:1803.01271*, 2018.
- Bengio, Y., Léonard, N., and Courville, A. Estimating or propagating gradients through stochastic neurons for conditional computation. *arXiv preprint arXiv:1308.3432*, 2013.
- Choromanski, K., Likhoshesterov, V., Dohan, D., Song, X., Gane, A., Sarlos, T., Hawkins, P., Davis, J., Mohiuddin, A., Kaiser, L., et al. Rethinking attention with performers. *arXiv preprint arXiv:2009.14794*, 2020.
- Conneau, A., Schwenk, H., Barrault, L., and Lecun, Y. Very deep convolutional networks for text classification. *arXiv preprint arXiv:1606.01781*, 2016.
- Dhariwal, P. and Nichol, A. Diffusion models beat gans on image synthesis. *Advances in Neural Information Processing Systems*, 34:8780–8794, 2021.
- Fang, J., Sun, Y., Zhang, Q., Li, Y., Liu, W., and Wang, X. Densely connected search space for more flexible neural architecture search. In *Proceedings of the IEEE/CVF conference on computer vision and pattern recognition*, pp. 10628–10637, 2020.
- Ghodrati, A., Bejnordi, B. E., and Habibiyan, A. Frameexit: Conditional early exiting for efficient video recognition. In *Proceedings of the IEEE/CVF Conference on Computer Vision and Pattern Recognition*, pp. 15608–15618, 2021.
- Gu, A., Goel, K., and Ré, C. Efficiently modeling long sequences with structured state spaces. *arXiv preprint arXiv:2111.00396*, 2021.
- Gu, A., Gupta, A., Goel, K., and Ré, C. On the parameterization and initialization of diagonal state space models. *arXiv preprint arXiv:2206.11893*, 2022.
- He, K., Zhang, X., Ren, S., and Sun, J. Deep residual learning for image recognition. In *Proceedings of the IEEE conference on computer vision and pattern recognition*, pp. 770–778, 2016.
- Hendrycks, D. and Gimpel, K. Gaussian error linear units (gelus). *arXiv preprint arXiv:1606.08415*, 2016.
- Huang, G., Liu, Z., Van Der Maaten, L., and Weinberger, K. Q. Densely connected convolutional networks. In *Proceedings of the IEEE conference on computer vision and pattern recognition*, pp. 4700–4708, 2017.
- Ioffe, S. and Szegedy, C. Batch normalization: Accelerating deep network training by reducing internal covariate shift. In *International conference on machine learning*, pp. 448–456. pmlr, 2015.
- Jaegle, A., Gimeno, F., Brock, A., Vinyals, O., Zisserman, A., and Carreira, J. Perceiver: General perception with iterative attention. In *International conference on machine learning*, pp. 4651–4664. PMLR, 2021.
- Kandasamy, K., Neiswanger, W., Schneider, J., Póczos, B., and Xing, E. P. Neural architecture search with bayesian optimisation and optimal transport. In Bengio, S., Wallach, H. M., Larochelle, H., Grauman, K., Cesa-Bianchi, N., and Garnett, R. (eds.), *Advances in Neural Information Processing Systems 31: Annual Conference on Neural Information Processing Systems 2018, NeurIPS 2018, December 3-8, 2018, Montréal, Canada*, pp. 2020–2029, 2018. URL <https://proceedings.neurips.cc/paper/2018/hash/f33ba15effa5c10e873bf3842afb46a6-Abstract.html>.
- Karras, T., Aittala, M., Laine, S., Härkönen, E., Hellsten, J., Lehtinen, J., and Aila, T. Alias-free generative adversarial networks. *Advances in Neural Information Processing Systems*, 34:852–863, 2021.
- Kietzmann, T. C., Spoerer, C. J., Sörensen, L. K., Cichy, R. M., Hauk, O., and Kriegeskorte, N. Recurrence is required to capture the representational dynamics of the human visual system. *Proceedings of the National Academy of Sciences*, 116(43):21854–21863, 2019.
- Kitaev, N., Kaiser, Ł., and Levskaya, A. Reformer: The efficient transformer. *arXiv preprint arXiv:2001.04451*, 2020.
- Krizhevsky, A., Hinton, G., et al. Learning multiple layers of features from tiny images. 2009.
- Krizhevsky, A., Sutskever, I., and Hinton, G. E. Imagenet classification with deep convolutional neural networks. In Pereira, F., Burges, C., Bottou, L., and Weinberger, K. (eds.), *Advances in Neural Information Processing Systems*, volume 25. Curran Associates, Inc., 2012. URL <https://proceedings.neurips.cc/paper/2012/file/c399862d3b9d6b76c8436e924a68c45b-Paper.pdf>.
- LeCun, Y., Bottou, L., Bengio, Y., and Haffner, P. Gradient-based learning applied to document recognition. *Proceedings of the IEEE*, 86(11):2278–2324, 1998.
- Lee-Thorp, J., Ainslie, J., Eckstein, I., and Ontanon, S. Fnet: Mixing tokens with fourier transforms. *arXiv preprint arXiv:2105.03824*, 2021.

- Li, Z., Kovachki, N., Azizzadenesheli, K., Liu, B., Bhattacharya, K., Stuart, A., and Anandkumar, A. Fourier neural operator for parametric partial differential equations. *arXiv preprint arXiv:2010.08895*, 2020.
- Linsley, D., Kim, J., Veerabadran, V., Windolf, C., and Serre, T. Learning long-range spatial dependencies with horizontal gated recurrent units. *Advances in neural information processing systems*, 31, 2018.
- Liu, C., Chen, L.-C., Schroff, F., Adam, H., Hua, W., Yuille, A. L., and Fei-Fei, L. Auto-deeplab: Hierarchical neural architecture search for semantic image segmentation. In *Proceedings of the IEEE/CVF conference on computer vision and pattern recognition*, pp. 82–92, 2019.
- Liu, H., Simonyan, K., Vinyals, O., Fernando, C., and Kavukcuoglu, K. Hierarchical representations for efficient architecture search. In *6th International Conference on Learning Representations, ICLR 2018, Vancouver, BC, Canada, April 30 - May 3, 2018, Conference Track Proceedings*. OpenReview.net, 2018a. URL <https://openreview.net/forum?id=BJQRKzbA->.
- Liu, H., Simonyan, K., and Yang, Y. Darts: Differentiable architecture search. *arXiv preprint arXiv:1806.09055*, 2018b.
- Loshchilov, I. and Hutter, F. Sgdr: Stochastic gradient descent with warm restarts. *arXiv preprint arXiv:1608.03983*, 2016.
- Loshchilov, I. and Hutter, F. Decoupled weight decay regularization. *arXiv preprint arXiv:1711.05101*, 2017.
- Ma, X., Kong, X., Wang, S., Zhou, C., May, J., Ma, H., and Zettlemoyer, L. Luna: Linear unified nested attention. *Advances in Neural Information Processing Systems*, 34: 2441–2453, 2021.
- Ma, X., Zhou, C., Kong, X., He, J., Gui, L., Neubig, G., May, J., and Zettlemoyer, L. Mega: moving average equipped gated attention. *arXiv preprint arXiv:2209.10655*, 2022.
- Maas, A., Daly, R. E., Pham, P. T., Huang, D., Ng, A. Y., and Potts, C. Learning word vectors for sentiment analysis. In *Proceedings of the 49th annual meeting of the association for computational linguistics: Human language technologies*, pp. 142–150, 2011.
- Nangia, N. and Bowman, S. R. Listops: A diagnostic dataset for latent tree learning. *arXiv preprint arXiv:1804.06028*, 2018.
- Oord, A. v. d., Dieleman, S., Zen, H., Simonyan, K., Vinyals, O., Graves, A., Kalchbrenner, N., Senior, A., and Kavukcuoglu, K. Wavenet: A generative model for raw audio. *arXiv preprint arXiv:1609.03499*, 2016.
- Radev, D. R., Muthukrishnan, P., Qazvinian, V., and Abu-Jbara, A. The acl anthology network corpus. *Language Resources and Evaluation*, 47(4):919–944, 2013.
- Riad, R., Teboul, O., Grangier, D., and Zeghidour, N. Learning strides in convolutional neural networks. *arXiv preprint arXiv:2202.01653*, 2022.
- Romero, D. W., Brintjes, R.-J., Tomczak, J. M., Bekkers, E. J., Hoogendoorn, M., and van Gemert, J. C. Flexconv: Continuous kernel convolutions with differentiable kernel sizes. *arXiv preprint arXiv:2110.08059*, 2021a.
- Romero, D. W., Kuzina, A., Bekkers, E. J., Tomczak, J. M., and Hoogendoorn, M. Ckconv: Continuous kernel convolution for sequential data. *arXiv preprint arXiv:2102.02611*, 2021b.
- Romero, D. W., Knigge, D. M., Gu, A., Bekkers, E. J., Gavves, E., Tomczak, J. M., and Hoogendoorn, M. Towards a general purpose cnn for long range dependencies in nd. *arXiv preprint arXiv:2206.03398*, 2022.
- Romero, D. W., Knigge, D. M., Gu, A., Bekkers, E. J., Gavves, E., Tomczak, J. M., Hoogendoorn, M., and Sonke, J.-J. Modelling long range dependencies in nd: From task-specific to a general purpose CNN. In *Submitted to The Eleventh International Conference on Learning Representations*, 2023. URL <https://openreview.net/forum?id=ZW5aK4yCRqU>. under review.
- Ronneberger, O., Fischer, P., and Brox, T. U-net: Convolutional networks for biomedical image segmentation. In *International Conference on Medical image computing and computer-assisted intervention*, pp. 234–241. Springer, 2015.
- Schuster, T., Fisch, A., Gupta, J., Dehghani, M., Bahri, D., Tran, V. Q., Tay, Y., and Metzler, D. Confident adaptive language modeling. *arXiv preprint arXiv:2207.07061*, 2022.
- Sercu, T., Puhersch, C., Kingsbury, B., and LeCun, Y. Very deep multilingual convolutional neural networks for lvcsr. In *2016 IEEE international conference on acoustics, speech and signal processing (ICASSP)*, pp. 4955–4959. IEEE, 2016.
- Shen, J., Khodak, M., and Talwalkar, A. Efficient architecture search for diverse tasks. *arXiv preprint arXiv:2204.07554*, 2022.
- Sitzmann, V., Martel, J., Bergman, A., Lindell, D., and Wetzstein, G. Implicit neural representations with periodic activation functions. *Advances in Neural Information Processing Systems*, 33:7462–7473, 2020.

- Smith, J. T., Warrington, A., and Linderman, S. W. Simplified state space layers for sequence modeling. *arXiv preprint arXiv:2208.04933*, 2022.
- Srivastava, N., Hinton, G., Krizhevsky, A., Sutskever, I., and Salakhutdinov, R. Dropout: a simple way to prevent neural networks from overfitting. *The journal of machine learning research*, 15(1):1929–1958, 2014.
- Tancik, M., Srinivasan, P., Mildenhall, B., Fridovich-Keil, S., Raghavan, N., Singhal, U., Ramamoorthi, R., Barron, J., and Ng, R. Fourier features let networks learn high frequency functions in low dimensional domains. *Advances in Neural Information Processing Systems*, 33: 7537–7547, 2020.
- Tay, Y., Dehghani, M., Abnar, S., Shen, Y., Bahri, D., Pham, P., Rao, J., Yang, L., Ruder, S., and Metzler, D. Long range arena: A benchmark for efficient transformers. *arXiv preprint arXiv:2011.04006*, 2020.
- Teerapittayanon, S., McDanel, B., and Kung, H.-T. Branchynet: Fast inference via early exiting from deep neural networks. In *2016 23rd International Conference on Pattern Recognition (ICPR)*, pp. 2464–2469. IEEE, 2016.
- Tu, R., Roberts, N., Khodak, M., Shen, J., Sala, F., and Talwalkar, A. Nas-bench-360: Benchmarking neural architecture search on diverse tasks. In *Thirty-sixth Conference on Neural Information Processing Systems Datasets and Benchmarks Track*, 2022.
- Vaswani, A., Shazeer, N., Parmar, N., Uszkoreit, J., Jones, L., Gomez, A. N., Kaiser, Ł., and Polosukhin, I. Attention is all you need. *Advances in neural information processing systems*, 30, 2017.
- Zagoruyko, S. and Komodakis, N. Wide residual networks. *arXiv preprint arXiv:1605.07146*, 2016.
- Zaheer, M., Guruganesh, G., Dubey, K. A., Ainslie, J., Alberti, C., Ontanon, S., Pham, P., Ravula, A., Wang, Q., Yang, L., et al. Big bird: Transformers for longer sequences. *Advances in Neural Information Processing Systems*, 33:17283–17297, 2020.
- Zeghidour, N., Xu, Q., Liptchinsky, V., Usunier, N., Synnaeve, G., and Collobert, R. Fully convolutional speech recognition. *arXiv preprint arXiv:1812.06864*, 2018.
- Zhang, K. and Bloom, J. S. deepcr: cosmic ray rejection with deep learning. *The Astrophysical Journal*, 889(1): 24, 2020.
- Zhang, R. Making convolutional networks shift-invariant again. In *International conference on machine learning*, pp. 7324–7334. PMLR, 2019.
- Zoph, B. and Le, Q. V. Neural architecture search with reinforcement learning. In *5th International Conference on Learning Representations, ICLR 2017, Toulon, France, April 24-26, 2017, Conference Track Proceedings*. OpenReview.net, 2017. URL <https://openreview.net/forum?id=r1Ue8Hcxg>.

Appendix

A. Architectures Found by DNArch

Table 4. Architectures found by DNArch for the LRA benchmark.

TASK	DEPTH	KERNEL SIZE	RESOLUTION	WIDTH [N _{in} , N _{mid} , N _{out}]
LISTOPS	8	266	2048	[150 189 145]
		569	632	[150 168 168]
		1401	1416	[176 186 162]
		310	310	[166 175 153]
		213	213	[154 159 163]
		12	301	[168 128 162]
		5	250	[170 158 153]
		24	502	[153 171 165]
TEXT	8	445	2284	[180 217 205]
		691	2939	[208 176 153]
		1420	1420	[152 152 120]
		415	1313	[120 120 147]
		1467	1467	[147 118 135]
		52	594	[134 173 153]
RETRIEVAL	8	101	932	[150 156 183]
		149	1036	[180 92 192]
		2	1913	[29 33 172]
		136	2058	[184 174 183]
		1013	2363	[205 171 161]
		1446	2724	[188 164 115]
IMAGE	8	7	2604	[29 29 163]
		1	2756	[29 35 154]
		6	3545	[71 110 147]
		1	3899	[71 88 137]
		203	1024	[118 155 147]
		279	1024	[146 172 164]
		219	486	[173 166 196]
		308	308	[199 197 196]
PATHFINDER	8	144	144	[207 197 92]
		8	125	[106 29 75]
		30	96	[78 28 110]
		40	126	[104 51 104]
		195	1024	[109 140 171]
		493	770	[171 168 158]
		418	507	[144 183 170]
		318	318	[173 187 178]
PATH-X	5	236	236	[182 162 160]
		231	231	[161 121 103]
		8	251	[105 47 210]
		4	253	[116 29 188]
		2484	15331	[280 174 157]
		7204	7204	[177 280 159]
3669	3772	[167 280 98]		
2323	5496	[123 164 164]		
513	4768	[136 128 195]		

B. Learning downsampling in the spatial Domain

Differentiable Masking learns downsampling by multiplying the spectrum $\tilde{f}=\mathcal{F}[f]$ of a signal f with a differentiable mask $m(\cdot; \theta)$, and cropping the output above the cutoff frequency of the mask ω_{\max} next. However, it is not necessary to perform this operation in the Fourier domain. Downsampling can also be learned directly in the spatial domain.

The *Fourier convolution theorem* states that the spatial convolution is equivalent to a pointwise multiplication in the Fourier domain. However, this equivalence works in both directions. That is, we can equivalently say that the pointwise multiplication on the Fourier domain is equal to a

Table 5. Architectures found by DNArch for 2D datasets.

TASK	DEPTH	KERNEL SIZE [Y X]	RESOLUTION [Y X]	WIDTH [N _{in} , N _{mid} , N _{out}]
IMAGE CLASSIFICATION TASKS				
CIFAR10	8	[9 7]	[32 32]	[142 139 145]
		[12 8]	[32 32]	[145 160 157]
		[25 7]	[32 20]	[158 186 182]
		[9 10]	[9 15]	[186 208 168]
		[1 13]	[5 15]	[169 177 150]
		[1 10]	[6 11]	[151 139 156]
CIFAR100	8	[5 1]	[15 4]	[154 115 110]
		[6 5]	[11 7]	[108 41 166]
		[13 7]	[32 32]	[104 107 116]
		[6 10]	[32 32]	[114 134 134]
		[11 8]	[22 22]	[139 192 166]
		[13 7]	[16 18]	[173 201 197]
DARCY FLOW	3	[8 12]	[10 12]	[205 251 51]
		[1 1]	[8 9]	[62 56 157]
		[5 9]	[8 10]	[162 175 254]
		[8 7]	[9 9]	[280 280 280]
		[43 38]	[80 72]	[156 280 107]
		[22 22]	[22 22]	[180 204 78]
COSMIC	6	[76 76]	[85 85]	[280 280 50]
		[94 111]	[128 128]	[18 110 23]
		[2 13]	[20 45]	[186 207 139]
		[129 129]	[129 129]	[126 265 100]
		[129 121]	[129 129]	[78 105 59]
		[90 89]	[129 129]	[57 201 197]
[76 74]	[76 74]	202 145 216]		

convolution on the spatial domain. Consequently, we can represent the pointwise multiplication of the spectrum of the input $\mathcal{F}[f]$ and the differentiable mask $m(\cdot; \theta)$ as the convolution of their inverse Fourier transforms. Formally:

$$\begin{aligned}
 \tilde{f} \cdot m(\cdot; \theta) &= \mathcal{F}[\mathcal{F}^{-1}[\tilde{f}] * \mathcal{F}^{-1}[m(\cdot; \theta)]] \\
 &= \mathcal{F}[\mathcal{F}^{-1}[\mathcal{F}[f]] * \mathcal{F}^{-1}[m(\cdot; \theta)]] \\
 &= \mathcal{F}[f * \mathcal{F}^{-1}[m(\cdot; \theta)]] \quad (12)
 \end{aligned}$$

In other words, we can perform the same operation in the spatial domain by convolution the original input signal f with the inverse Fourier transform of the mask $m(\cdot; \theta)$.

Defining the output resolution. Eq. 12 defines how low-pass filtering can be performed on the spatial domain, but it does not provide information regarding the final resolution of the operation. To derive the resolution of the output, we can simply use Eqs. 9, 10 to analytically derive the size of the mask. Once the size of the mask is derived, we can simply take the downsampled signal –after using Eq. 12–, and downsample it to match the size of the mask.

C. Computational complexity of masked network components

In this section, we derive the computational complexity of all layers used in the CCNN architecture with and without the use of masks. The calculation of these complexities follows the same reasoning as the pointwise linear layer provided as example in the main text.

With L , N_{in} and N_{out} the length, number of input chan-

nels and number of output channels of a given layer, and $\text{size}(m_{\text{res}})$, $\text{size}(m_{N_{\text{in}}})$, $\text{size}(m_{N_{\text{out}}})$ the size of the masks along the corresponding dimensions, the complexity of the layers used in the CCNN architectures are given by:

Pointwise linear layer:

$$C_{\text{lin}}(f) = L \cdot N_{\text{in}} \cdot N_{\text{out}}$$

$$C_{\text{lin,masked}} = \text{size}(m_{\text{res}}) \cdot \text{size}(m_{N_{\text{in}}}) \cdot \text{size}(m_{N_{\text{out}}})$$

Fourier convolution:

$$C_{\mathcal{F}\text{conv}} = L \log(L)$$

$$C_{\mathcal{F}\text{conv,masked}} = \text{size}(m_{\text{res}}) \log(\text{size}(m_{\text{res}}))$$

Pointwise operations –GELU, Dropout, etc.–:

$$C_{\text{pointwise}} = L \cdot N_{\text{in}}$$

$$C_{\text{pointwise,masked}} = \text{size}(m_{\text{res}}) \cdot \text{size}(m_{N_{\text{in}}})$$

D. Dataset descriptions

D.1. The Long Range Arena benchmark

The Long Range Arena (Tay et al., 2020) consists of six sequence modelling tasks with sequence lengths ranging from 1024 to over 16000. It encompasses modalities and objectives that require similarity, structural, and visuospatial reasoning. We follow the data preprocessing steps of Gu et al. (2021), which we also include here for completeness.

ListOps. An extended version of the dataset presented by Nangia & Bowman (2018). The task involves computing the integer result in the range zero to nine of a mathematical expression represented in prefix notation with brackets, e.g., $[\text{MAX}29[\text{MIN}47]0] \rightarrow 9$. Characters are encoded as one-hot vectors, with 17 unique values possible (opening brackets and operators are grouped into a single token). The sequences are of unequal length. Hence, the end of shorter sequences is padded with a fixed indicator value to a maximum length of 2048. The task has 10 different classes representing the possible integer results of the expression. It consists of 96K training sequences, 2K validation sequences, and 2K test sequences. No data normalization is applied.

Text. Based on the IMDB sentiment analysis dataset presented by Maas et al. (2011), the task is to classify movie reviews as having a positive or negative sentiment. The reviews are presented as a sequence of 129 unique integer tokens padded to a maximum length of 4096. The dataset contains 25K training sequences and 25K test sequences. No validation set is provided. No data normalization is applied.

Retrieval. Based on the ACL Anthology network corpus presented by Radev et al. (2013), the task is to classify whether two given textual citations are equivalent. To accomplish this, each citation is separately passed through an encoder, and passed to a final classifier layer. Denoting X_1 as the encoding for the first document and X_2 as the encoding for the second document, four features are created

and concatenated together as:

$$X = [X_1, X_2, X_1 \times X_2, X_1 - X_2],$$

which are subsequently passed to a two layered MLP. The goal of the task is to evaluate how well the network can represent the text by evaluating if the two citations are equivalent or not. Characters are encoded into a one-hot vector with 97 unique values and sequences are padded to a maximum length of 4000. The dataset includes 147.086 training pairs, 18.090 validation pairs, and 17.437 test pairs. No normalization is applied.

Image. The Image task uses 32×32 images of the CIFAR10 dataset (Krizhevsky et al., 2009). It views the images as sequences of length 1024 that correspond to a one-dimensional raster scan of the image. There are a total of 10 classes, 45K training examples, 5K validation examples and 10K test examples. The RGB pixel values are converted to grayscale intensities and then normalized to have zero mean and unit variance across the entire dataset.

PathFinder. Based on the PathFinder challenge introduced by Linsley et al. (2018), the task presents a 32×32 grayscale image with an start and an end point depicted as small circles. The task is to classify whether there is a dashed line (or path) joining the start and end points while presenting the input as a one-dimension raster scan of the image, alike the Image task. The dataset includes 160K training examples, 20K validation examples and 20K test examples. The input data is normalized to be in the range $[-1, 1]$.

Path-X. Path-X is an “extreme” version of the PathFinder dataset, in which the input images are of size 128×128 . As a result, the input sequences are sixteen times longer with a total length of 16384. Aside from this difference, the task is identical to the PathFinder dataset.

D.2. Image classification datasets

CIFAR10 and CIFAR100. The CIFAR10 dataset (Krizhevsky et al., 2009) consists of 60K real-world 32×32 RGB images uniformly drawn from 10 classes divided into training and test sets of 50K and 10K samples, respectively. The CIFAR100 dataset (Krizhevsky et al., 2009) is similar to the CIFAR10 dataset, with the difference that the images are uniformly drawn from 100 different classes. For validation purposes, we divide the training dataset of both CIFAR10 and CIFAR100 into training and validation sets of 45K and 5K samples, respectively. Both datasets are normalized to have zero mean and unit variance across the entire dataset.

D.3. NAS-Bench-360

NAS-Bench-360 (Tu et al., 2022) is a benchmark suite to evaluate Neural Architecture Search methods beyond image classification. The benchmark is composed of ten tasks spanning a diverse array of application domains, dataset sizes, problem dimensionalities, and learning objectives. In this

work, we consider two tasks from the NAS-Bench-360 suite which require dense predictions: The DarcyFlow (Li et al., 2020) and Cosmic (Zhang & Bloom, 2020) datasets.

DarcyFlow: Solving Partial Differential Equations. DarcyFlow aims to solve Partial Differential Equation (PDE) by using neural networks as a replacement for traditional solvers. The input for this task is a 85×85 grid specifying the initial conditions and coordinates of a fluid, and the output is a 2D grid of the same dimensions representing the fluid state at a later time. The ground truth for this task is the result computed by a traditional solver, and the objective is to minimize the Mean Squared Error (MSE) between the predicted fluid state and the ground truth.

Cosmic: Identifying Cosmic Ray Contamination. The Cosmic task involves identifying and masking corruption caused by charged particles collectively referred to as “cosmic rays” on images taken from space-based facilities. It uses imaging data of local resolved galaxies collected from the Gubble Space Telescope. The input is an 128×128 image corresponding to the artifact of cosmic rays, and the output is a 2D grid of the same dimensions predicting whether each pixel in the input is an artifact of cosmic rays. We report the false-negative rate of identification results.

E. Experimental details

E.1. General remarks

Code. Our code is written in JAX and our experiments are conducted on TPUs and GPUs. As outlined in the Limitations (Sec. 4), JAX and TPU training prevent DNArch from performing operations that change the dimensions of arrays during training. In addition to our JAX implementation, we will also release a PyTorch implementation of DNArch that supports these operations. We hope that this implementation will make DNArch more flexible and accessible, especially in scenarios where it is crucial to keep candidate networks close to the target complexity during the course of training.

The Continuous CNN and the CCNN residual block. The CCNN architecture is shown in Fig. 5. It is composed by an Encoder, a Decoder, and a number of CCNN residual blocks ResBlock (Romero et al., 2023). The Encoder is defined as a sequence of [PWLinear, BatchNorm (Ioffe & Szegedy, 2015), GELU (Hendrycks & Gimpel, 2016)] layers. For tasks dealing with text, we additionally utilize an Embedding layer mapping each token in the vocabulary to a vector representation of length equal to that used by Gu et al. (2021) (see Appx. D.1). For dense prediction tasks, the Decoder is a PWLinear layer, which is preceded by GlobalAvgPooling for global prediction tasks.

Batch Normalization in DNArch. As the architecture is constantly changing during the search process, we use batch-specific statistics for batch normalization instead of the

global moving average. This approach was adopted after early experiments showed that using the global moving average leads to a significant discrepancy in the behavior of the validation and training curves. Specifically, we observed that while the training curves were converging to a good solution, the validation curves resembled random predictions. This issue was resolved by deactivating the global moving average in Batch Normalization layers.

Continuous convolutional kernels MLP_ψ . We parameterize our convolutional kernels as a 4-layer MLP with 128 hidden units and a Fourier Encoding (Tancik et al., 2020) of the form $\gamma(\mathbf{x}) = [\cos(2\pi\omega_0 \mathbf{W}\mathbf{x}), \sin(2\pi\omega_0 \mathbf{W}\mathbf{x})]$, with $\mathbf{W} \in \mathbb{R}^{D \times 128}$ and ω_0 a hyperparameter that acts as a prior on the frequency content of the kernels (Romero et al., 2021b; Sitzmann et al., 2020). In contrast to Romero et al. (2021b), we utilize a single larger MLP_ψ to generate the kernels of the entire network. This allows the network MLP_ψ to administer its capacity across all layers. Using different MLP_ψ ’s for each layer as Romero et al. (2021b) is inadequate in the learnable architectures setting as some layers can be entirely erased. With our proposed solution, the capacity of the otherwise zeroed-out MLP_ψ is used to generate the kernels of the remaining layers.

Normalized relative positions. Following Romero et al. (2021b;a), we normalize the coordinates going into MLP_ψ to lie in the space $[-1, 1]^D$ for D-dimensional kernels.

Parameters and hyperparameters of the differentiable masks. We learn some of the parameters of the masks, and leave the others constant or treat them as a hyperparameter. Specifically, for Gaussian masks, we only learn their width, i.e., σ , and fix its mean to zero. For Sigmoid masks, we learn their offset μ and treat their temperature τ as a hyperparameter. For more information regarding the values of τ used in our parameter tuning step, please refer to Appx. E.2.

Maximum and minimum allowable sizes for the learnable differentiable masks. We define some minimum and maximum allowable sizes for the mask parameters, and reset them to these values after each training iteration if the updated parameter values lie outside that range. For the Gaussian mask, we constraint the minimum admissible value of σ such that the length of the corresponding dimension never collapses to a value of 1. This is to prevent the corresponding dimension to collapse such that it can grow afterwards if required. The minimum value depends on the resolution of the corresponding dimension, e.g., the maximum size of the convolutional kernel, and can be easily calculated with Eq. 3.

Note that the offset value of the Sigmoid mask μ could in principle assume any value in \mathbb{R} . However, if not controlled, μ could become too small and mask all values along a particular dimension to zero. Similarly, if μ is too large,

the gradient of the mask at all positions would become very small and it would be difficult to update the mask. To avoid these situations, we define minimum and maximum values of μ such that for the lowest value, the mask at the lowest position is equal to 0.95, and for the largest value, the mask at the highest position is equal to 0.85. These values are dependent on the value of the mask temperature τ , and can be easily calculated with Eq. 4.

Limiting the size of the mask to the maximum allowable ranges. As outlined in the Limitations (Sec. 4), we must set a maximum allowable size for the width and depth of the network on JAX. However, the maximum allowed value for the parameters of the masks (see previous paragraph) allows both masks to grow beyond the point on which the theoretical size of the masks is equal to the maximum allowable network size. For instance, for the maximum allowed parameter values of a Sigmoid mask, the last channel, i.e., the 280-th channel, would be weighted by a factor of 0.85. Consequently, the theoretical size of the mask as calculated by Eq. 10 will be well beyond 280. This value would lead to an unrealistic theoretical computational complexity that surpasses the real computational complexity the CCNN used.

To overcome this issue, we limit the maximum size of the mask calculated by Eq. 10 to be less or equal than the maximum allowable size, e.g., $\text{size}(m) = \min(\text{size}(m), 280)$. It is important to note, however, that clipping the value of size directly would stop the gradient flow for parameter values leading to sizes larger than 280. As a result, once the maximum size is reached, the mask would not be able to contract anymore. We avoid gradient flow stop by using clipping in combination with a straight-through estimator (Bengio et al., 2013). As a result, we are able to propagate the gradient across the clipping operation, and the resulting mask can still be modified even in the cropping operation is used.

E.2. Hyperparameters and training configurations

In this section, we include more information about the found hyperparameters, the values that were considered during hyperparameter tuning, and other training settings. The final hyperparameters used are listed in Table 6.

Optimizer, learning rates and learning rate schedule.

All our models are optimized with AdamW (Loshchilov & Hutter, 2017) in combination with a cosine annealing learning rate scheduler (Loshchilov & Hutter, 2016), and a linear learning rate warm-up stage of 10 epochs, except for ListOps, Retrieval and Path-X for which we have a warm-up stage of 5 epochs.

Regularization. We utilize dropout (Srivastava et al., 2014) –as shown in Fig. 5– as well as weight decay during training.

E.2.1. HYPERPARAMETER TUNING

Frequency prior ω_0 . The possible ω_0 values explored in this work are [1, 500, 1500, 2500, ...28500, 29500, 30000].

Tuning the value of λ . λ plays the role of controlling the weight of the computational loss $\mathcal{L}_{\text{comp}}$ relative to the task objective loss \mathcal{L}_{obj} . In this work, we find two settings which require different values of λ . One, given by the tasks that converge to a low prediction values relative to perfection, i.e., ListOps and CIFAR100, and for which the loss \mathcal{L}_{obj} remains relatively high at the end of training. The other group is given by all the other tasks, which converge to high prediction values –many even obtaining a perfect accuracy on the train set–, and for which \mathcal{L}_{obj} converges to values close to zero. For the first group, we require a higher value of λ such that the computational complexity loss $\mathcal{L}_{\text{comp}}$ remains relevant to the optimization objective. The final values of λ used are 5.0 and 0.1, respectively.

Tuning the temperature of the Sigmoid masks τ . For the resolution mask, we consider three values of τ , [25, 50, 100] which correspond to a minimum size of 10%, 5% and 2.5% of the corresponding dimension. For the channel mask, we consider two values $\tau \in [25, 50]$ which correspond to a minimum size of 10% and 5% of the corresponding dimension, but observe early during tuning that models prefer $\tau=25$. For the depth dimension, which is much more sparse than the channel and resolution dimensions, we consider two values $\tau \in [8, 16]$, which result on a minimum depth of 2 and 1 layers, respectively. We observe early during tuning that models prefer $\tau=8$.

Learning rate. The possible learning rate values explored in this work are [0.0001, 0.0005, 0.001, 0.005, 0.01, 0.02].

Dropout. The possible dropout values explored in this work are [0.0, 0.1, 0.2, 0.3].

Weight decay. The possible weight decay values considered in this work are [0.0, 0.0001, 0.001, 0.01, 0.05].

Table 6. Hyperparameters used for the reported results.

DATASET	EPOCHS	BATCH SIZE	LEARNING RATE	DROPOUT	WEIGHT DECAY	ω_0	λ	$\tau_{\text{resolution}}$	τ_{channel}	τ_{depth}
LISTOPS	50	50	0.005	0.0	0.01	27.5k	5.0	50	25	8
TEXT	100	50	0.02	0.2	0.01	19.5k	0.1	50	25	8
RETRIEVAL	50	50	0.001	0.1	0.01	21.5k	0.1	50	25	8
IMAGE	210	50	0.02	0.1	0.001	12.5k	0.1	25	25	8
PATHFINDER	210	50	0.005	0.0	0.001	21.5k	0.1	50	25	8
PATH-X	80	32	0.001	0.0	0.0	30k	0.1	100	25	8
CIFAR10	210	50	0.01	0.1	0.01	21.5k	0.1	25	25	8
CIFAR100	210	50	0.01	0.0	0.01	6.5k	5.0	25	25	8
DARCYFLOW	310	8	0.02	0.0	0.0001	24.5k	0.1	50	25	8
COSMIC	310	8	0.02	0.3	0.0001	5.5k	0.1	100	25	8